Journal of Luminescence 37 (1987) 9–20
North-Holland, Amsterdam

ENERGY TRANSFER BETWEEN Eu^{3+} IONS IN A LATTICE WITH TWO DIFFERENT CRYSTALLOGRAPHIC SITES: $Y_2O_3:Eu^{3+}$, $Gd_2O_3:Eu^{3+}$ and Eu_2O_3

M. BUIJS, A. MEYERINK and G. BLASSE

Solid State Department, Physical Laboratory, University of Utrecht, P.O. Box 80.000, 3508 TA Utrecht, The Netherlands

Received 23 September 1986
Accepted 9 December 1986

The Eu^{3+} ion occupies two different crystallographic sites in $(Y_{1-x}Eu_x)_2O_3$ and $(Gd_{1-x}Eu_x)_2O_3$, with site symmetry S_6 and C_2. Energy transfer over more than 7 Å occurs from Eu^{3+} (S_6) ions to Eu^{3+} (C_2) ions. This is shown to be a direct one-phonon assisted process, in combination with a one-site resonant two-phonon assisted process at higher temperatures. For $x = 1$ there is energy migration over the Eu^{3+} (C_2) sublattice to quenching impurities. The presence of cooperative absorption points to superexchange interaction between the Eu^{3+} ions.

1. Introduction

The effect of the peculiar structural properties of certain rare-earth compounds on the energy transfer processes in these systems has been a recent subject of research in our laboratory. We found that the one-dimensional character of the rare-earth sublattice in $EuMgB_5O_{10}$ [1] and $TbMgB_5O_{10}$ [2] can be recognized from the behaviour of the energy transfer in those systems. Having finished investigations on three-, two- and one-dimensional lattices with one type of Eu^{3+} ions [3], we have now turned our interest to compounds offering more than one site for the Eu^{3+} ion. In β'-$(Gd_{1-x}Eu_x)_2(MoO_4)_3$ the Eu^{3+} ion occupies two different crystallographic sites. For low Eu^{3+} concentrations energy transfer occurs between Eu^{3+} ions on these two sites, leading to energy migration with quasi-two-dimensional character for $x = 1$ [4]. The differences between the sites are very small and there is no observable energy difference between the $^5D_0$ levels of the Eu^{3+} ions on either site. Hence the energy transfer from one site to the other has the same probability as the back transfer, these levels being the ones involved as the excited states in the transfer process.

Cubic C-type Y_2O_3 doped with Eu^{3+} has also two crystallographically different rare-earth sites, but energy transfer between the Eu^{3+} ions will be different in this host lattice compared to transfer in the molybdate, because in Y_2O_3 the sites are strongly different, having site symmetries C_2 and S_6 [5]. The oxygen surroundings of these sites are given in fig. 1. The $^5D_0$ level of a Eu^{3+} ion on a S_6 site lies 87 cm^{-1} higher than the $^5D_0$ level of a Eu^{3+} (C_2) ion [6]. Even at low temperatures energy transfer was found to occur from Eu^{3+} (S_6) to Eu^{3+} (C_2) in spite of this large energy mismatch [5–10].

A considerable amount of investigations on the energy transfer process in $Y_2O_3:Eu^{3+}$ has been performed till now. Driving force behind these efforts is the use of this compound as a commercial phosphor [9,10]. But none of the investigations led to a complete unraveling of the processes in this compound. In some of them a model was used to describe the transfer process which did not take into account the distance dependence of the energy transfer probability [6–8]. Other studies were of a more qualitative nature [9,10].

The aim of this work is to find a more detailed description of the energy transfer processes in $Y_2O_3:Eu^{3+}$, $Gd_2O_3:Eu^{3+}$ and Eu_2O_3. These compounds have the same crystal structure. $Gd_2O_3:Eu^{3+}$ was chosen because it is essentially

0022-2313/87/$03.50

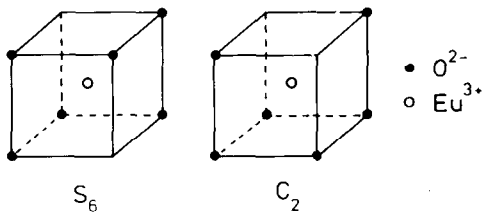

Fig. 1. Oxygen surroundings of the two rare-earth sites in Y_2O_3.

identical to $Y_2O_3:Eu^{3+}$, except for the ionic radii of the rare-earth ions. Eu^{3+} and Gd^{3+} have nearly the same radius, 0.95 Å and 0.94 Å, respectively, while Y^{3+} is smaller (0.90 Å) [11]. For pairs of neighbouring Eu^{3+} ions in $Y_2O_3:Eu^{3+}$ this leads to slight distortions in the crystal field [10]. The ions in these pairs have slightly displaced spectral lines, and in the case of a Eu^{3+} (S_6)–Eu^{3+} (C_2) pair the energy transfer from Eu^{3+} (S_6) to Eu^{3+} (C_2) is faster than for the rest of the Eu^{3+} (S_6) ions. In Gd_2O_3 the mutual proximity of the Eu^{3+} ions has no effect, since Eu^{3+} and Gd^{3+} have the same size. This allows an unambiguous analysis of the transfer processes in $Gd_2O_3:Eu^{3+}$ which are identical to the main processes in $Y_2O_3:Eu^{3+}$, without interference of pair effects.

Finally the transfer in the concentrated system Eu_2O_3 will be considered. Since each Eu^{3+} ion has a large number of Eu^{3+} neighbours at short distances [12], energy migration over the Eu^{3+} sublattice is very likely to occur.

2. Experimental

The measurements were performed on powders of composition $(Y_{1-x}Eu_x)_2O_3$ $(0 < x \leqslant 1)$ and $(Gd_{1-x}Eu_x)_2O_3$ $(x = 0.5\%, 5\%)$. The compounds were obtained by dissolving Eu_2O_3 (Highways 99.99%) and Y_2O_3 (Highways 99.999%) or Gd_2O_3 (Highways 99.999%) in nitric acid (Merck, p.a.grade). Mixed oxalates were precipitated by adding oxalic acid. After washing and drying, the precipitate was fired for 4 h at 1000°C. The resulting samples were checked by X-ray powder diffraction using CuKα radiation. To avoid contamination with impurities from the nitric acid, the Eu_2O_3 sample used for decay measurements was prepared by firing the starting material Eu_2O_3 for 4 h at 1000°C.

The experimental set-up is described in refs. [1,13]. Measurements were made in the temperature region from 1.3 K to 300 K.

3. Results

3.1. Spectral properties

The excitation spectrum of the Eu^{3+} emission in $(Y_{1-x}Eu_x)_2O_3$ and $(Gd_{1-x}Eu_x)_2O_3$ consists of the well-known sharp lines in the region 240 nm to 600 nm, corresponding to transitions within the $4f^6$ configuration of Eu^{3+} and of the O^{2-}–Eu^{3+} charge transfer band which peaks at about 250 nm. In the Gd^{3+} compounds also the Gd^{3+} $^8S \rightarrow {}^6I$ and $^8S \rightarrow {}^6P$ transitions occur due to energy transfer from Gd^{3+} to Eu^{3+}.

Upon closer examination, for instance in the $^7F_0 \rightarrow {}^5D_1$ region, a distinction can be made between lines belonging to the Eu^{3+} (S_6) ions and lines belonging to the Eu^{3+} (C_2) ions. The same holds for the emission spectrum, where emission lines occurring from the $^5D_0$ level of both types of Eu^{3+} ions are present. These spectra have been described in detail in refs. [5,9,10]. At very low Eu^{3+} concentrations weak lines occurring from the higher lying $^5D_1$ level can be observed. They disappear on increasing Eu^{3+} concentration due to cross relaxation [14].

There is no preferential occupation by the Eu^{3+} ions of the S_6 and C_2 sites, which are present in the ratio 1 : 3 [8]. Due to the presence of a center of symmetry, only magnetic transitions (selection rule $\Delta J = 0, \pm 1$, $J = 0 \rightarrow J = 0$ forbidden) are allowed for the Eu^{3+} (S_6) ion. Transitions of interest for this study are $^7F_0 \rightarrow {}^5D_1$ and $^5D_0 \rightarrow {}^7F_1$. Besides these magnetic dipole transitions, the Eu^{3+} (C_2) ion shows also forced electric dipole transitions, of which we will consider the $^7F_0 \rightleftarrows {}^5D_0$ and $^5D_0 \rightarrow {}^7F_2$ transitions.

The energy transfer from Eu^{3+} (S_6) to Eu^{3+} (C_2) is a very efficient process. Even in the compound $(Y_{0.995}Eu_{0.005})_2O_3$ at 4.2 K, the $^7F_0 \rightarrow {}^5D_1$ (S_6) lines occur in the excitation spectrum re-

corded by monitoring the $^5D_0 \rightarrow {}^7F_2$ (C_2) emission. This spectrum is given in fig. 2. The number of lines in this spectrum is in agreement with the site symmetries. The displacement of the spectral lines for paired Eu^{3+} ions mentioned in section 1 can be seen in fig. 2a, which gives the $^7F_0 \rightarrow {}^5D_{1b}$ (S_6) line in more detail. Besides the main line at 523.6 nm, two satellite lines occur belonging to Eu^{3+} (S_6) ions, which have a neighbouring Eu^{3+} (C_2) ion at 3.5 Å or 4.0 Å. These lines are rather intense because the corresponding Eu^{3+} (S_6) ions transfer their energy more efficiently to the Eu^{3+} (C_2) ions than the Eu^{3+} (S_6) ions belonging to the main line. That their presence is caused by the difference between the ionic radii of Y^{3+} and Eu^{3+}, can be seen in fig. 2b. It shows the same excitation line in $(Gd_{0.995}Eu_{0.005})_2O_3$. No satellite lines occur because Gd^{3+} and Eu^{3+} have nearly the same ionic radius.

The intensity ratio of Eu^{3+} (S_6) and Eu^{3+} (C_2) excitation lines in the $^7F_0 \rightarrow {}^5D_1$ region while monitoring the $^5D_0 \rightarrow {}^7F_2$ (C_2) emission increases on increasing Eu^{3+} concentration, indicating an increasing rate of transfer. Similarly the intensity ratio of Eu^{3+} (S_6) and Eu^{3+} (C_2) emission lines under excitation into one of the $^7F_0 \rightarrow {}^5D_1$ (S_6) lines decreases on increasing Eu^{3+} concentration. Figure 3 shows the emission spectrum of $(Gd_{0.95}Eu_{0.05})_2O_3$ after excitation into $^7F_0 \rightarrow {}^5D_{1b}$

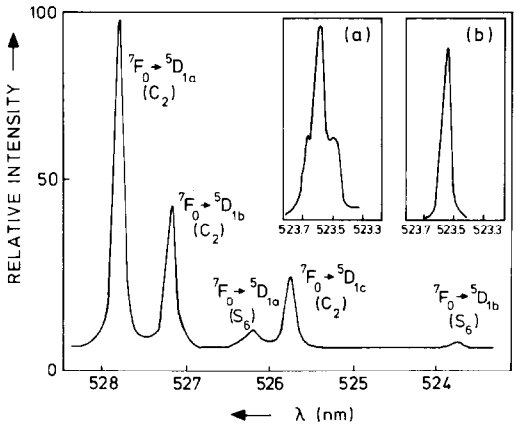

Fig. 2. Excitation spectrum in the $^7F_0 \rightarrow {}^5D_1$ region of $(Y_{0.995}Eu_{0.005})_2O_3$, recorded at 4.2 K (em. = 611.25 nm (C_2)). (a): magnification of $^7F_0 \rightarrow {}^5D_{1b}$ (S_6) line, (b): same line in same spectrum of $(Gd_{0.995}Eu_{0.005})_2O_3$.

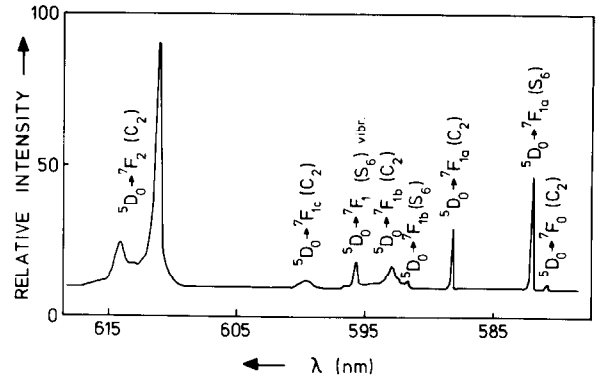

Fig. 3. Emission spectrum of $(Gd_{0.95}Eu_{0.05})_2O_3$, recorded at 4.2 K (exc. = 523.54 nm (S_6)).

(S_6) at 4.2 K. We follow the assignment given in ref. [10].Only 11% of the total emission intensity originates from the excited Eu^{3+} (S_6) ions. If one assumes the existence of a critical transfer distance R_0, for which holds that for any Eu^{3+} (S_6)–Eu^{3+} (C_2) pair the Eu^{3+} (S_6) ion will decay radiatively if their separation is more than R_0 and $S_6 \rightarrow C_2$ transfer will occur if it is less than R_0, an estimate of R_0 can be made using this value. It represents the amount of isolated, radiatively decaying Eu^{3+} (S_6) ions. If every Eu^{3+} (S_6) has n neighbouring sites within R_0 that can be occupied by a Eu^{3+} (C_2) ion, the probability for the Eu^{3+} (S_6) ion to be isolated in $(Gd_{0.95}Eu_{0.05})_2O_3$ is equal to 0.95^n. This is the probability for all n sites to be occupied by Gd^{3+}. When the amount of isolated Eu^{3+} (S_6) ions is 11%, it follows that $0.95^n = 0.11$, resulting in $n = 43$. Given the structural data of Gd_2O_3 [12], this means that R_0 has a value of about 8 Å at 4.2 K.

Energy transfer from Eu^{3+} (C_2) to Eu^{3+} (S_6) does not occur in $Y_2O_3:Eu^{3+}$ and $Gd_2O_3:Eu^{3+}$ at low temperatures. At 300 K some Eu^{3+} (S_6) emission can, however, be observed after excitation into Eu^{3+} (C_2), depending on the Eu^{3+} concentration. At these temperatures transfer from C_2 to S_6 becomes possible because the energy difference between the $^5D_0$ levels of both ions can be bridged thermally.

The positions of the excitation and emission lines in $Gd_2O_3:Eu^{3+}$ and Eu_2O_3 are slightly different from the positions in $Y_2O_3:Eu^{3+}$, due to

the difference of the ionic radii which leads to a slightly distorted crystal field. The scheme of the Eu^{3+} $^7F_{0,1}$ and $^5D_{0,1}$ levels in Gd_2O_3 and Eu_2O_3, derived from the present results, is given in fig. 4 for both sites. Since the only transitions allowed for the S_6 site are $^7F_0 \rightarrow {}^5D_1$ and $^5D_0 \rightarrow {}^7F_1$, additional information being either the $^7F_{1a}-{}^7F_0$ (S_6) or the $^5D_{1a}-{}^5D_0$ (S_6) energy difference is necessary to determine the position of the $^5D_0$ (S_6), level. The determination of the former will be discussed below.

In Eu_2O_3 the transfer from Eu^{3+} (S_6) to Eu^{3+} (C_2) has become very efficient: no Eu^{3+} (S_6) emission can be detected after excitation into Eu^{3+} (S_6). The emission spectra after excitation into both types of ions have become identical. Also inhomogeneous broadening of the lines occurs. The linewidth of the $^5D_0 \rightarrow {}^7F_0$ (C_2) transition is 6 cm^{-1} at 4.2 K compared to 1.5 cm^{-1} in $(Gd_{0.995}Eu_{0.005})_2O_3$ and 4 cm^{-1} in $(Gd_{0.95}Eu_{0.05})_2O_3$.

Another striking feature of the concentrated Eu_2O_3 system is the occurrence of seven additional lines at the high-energy side of the $^7F_0 \rightarrow {}^5D_1$ excitation spectrum while monitoring the $^5D_0 \rightarrow {}^7F_2$ (C_2) emission. This is illustrated in fig. 5. The energy difference between each of the lines indicated by "1" and the consecutive lines of the $^7F_0 \rightarrow {}^5D_1$ (C_2) transition is equal to the energy difference between each of the lines indicated by "2" and the consecutive lines of the $^7F_0 \rightarrow {}^5D_1$ (S_6) transition, viz. 216 cm^{-1}. This value corresponds to the $^7F_{1a}-{}^7F_0$ (C_2) energy difference, indicating that the additional lines are due to cooperative absorption by two Eu^{3+} ions. They can be denoted by

$$2\,{}^7F_0(C_2) \rightarrow {}^5D_1(C_2) + {}^7F_1(C_2), \qquad (1)$$

and

$$^7F_0(S_6) + {}^7F_0(C_2) \rightarrow {}^5D_1(S_6) + {}^7F_1(C_2). \qquad (2)$$

The energy difference between the first line indicated by "3" and the $^7F_0 \rightarrow {}^5D_{1a}$ (C_2) line is equal to the difference between the second "3" line and the $^7F_0 \rightarrow {}^5D_{1c}$ (C_2) line, viz. 139 cm^{-1}. Since this value is close to the $^7F_{1a}-{}^7F_0$ (S_6) energy difference in $Y_2O_3:Eu^{3+}$, being 132 cm^{-1} [6], these lines are described by the process

$$^7F_0(C_2) + {}^7F_0(S_6) \rightarrow {}^5D_1(C_2) + {}^7F_1(S_6). \qquad (3)$$

The third line belonging to this transition is hidden by the $^7F_0 \rightarrow {}^5D_{1b}$ (S_6) line. In this way the $^7F_{1a}-{}^7F_0$ (S_6) energy difference is determined to be 139 cm^{-1}. This value can be used to complete the energy level scheme given in fig. 4. No cooperative absorption between two Eu^{3+} (S_6) ions could be detected. This is to be expected since the distance between two Eu^{3+} (S_6) ions (5.4 Å) is much larger than the distance between two Eu^{3+} (C_2) ions (3.6 Å) or between a Eu^{3+} (S_6) and a Eu^{3+} (C_2) ion (3.6 Å).

Cooperative absorption lines of this intensity have been found before in other concentrated

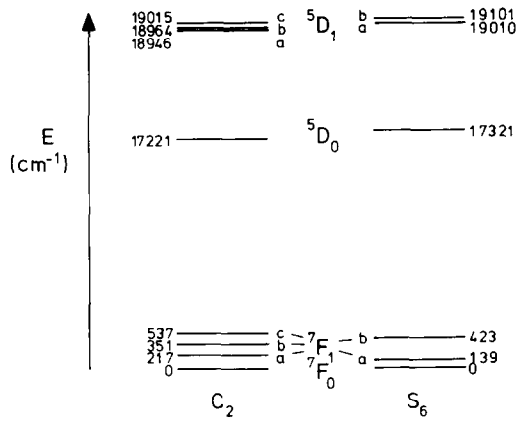

Fig. 4. Energy level diagram of Eu^{3+} on the two sites in Gd_2O_3 and Eu_2O_3. Only the $^7F_{0,1}$ and $^5D_{0,1}$ levels are shown.

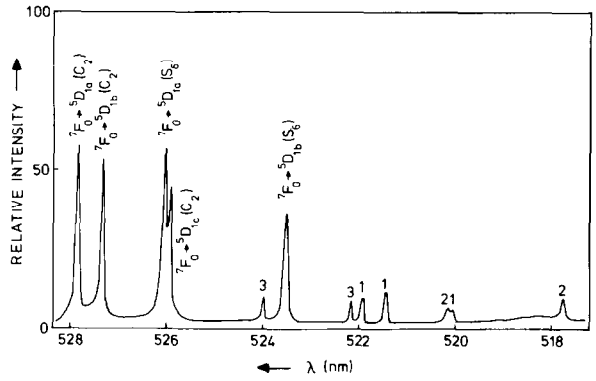

Fig. 5. Excitation spectrum in the $^7F_0 \rightarrow {}^5D_1$ region of Eu_2O_3, recorded at 4.2 K (em. = 611.3 nm (C_2)). 1, 2, 3: lines due to cooperative absorption (see text).

Eu^{3+} compounds, viz. Eu_2O_2S [15] and $Eu_2O_2SO_4$ [16]. It is, however, the first time that cooperative absorption is observed involving different Eu^{3+} ions. Imanaga et al. have argued that such a great intensity relative to the normal transitions cannot be explained by multipolar or direct exchange interactions between the Eu^{3+} ions. They explained it by assuming a superexchange mechanism via the charge transfer state. The relative intensity of the cooperative absorption lines with respect to the single ion lines in Eu_2O_2S is twice as large as in Eu_2O_3. This is consequently due to the fact that the charge transfer state in the oxysulphide lies at lower energies (28600 cm^{-1}) than in Eu_2O_3 (40000 cm^{-1}), which leads to a stronger superexchange interaction in the former. We found superexchange between Eu^{3+} ions in β'-$Gd_2(MoO_4)_3:Eu^{3+}$ [4]. However, no cooperative absorption could be detected.

3.2. Concentration dependence of the luminescence

In order to study the concentration quenching of the luminescence in $(Y_{1-x}Eu_x)_2O_3$ the integrated Eu^{3+} emission ($^5D_0 \rightarrow {}^7F_{0,1,2}$) after broad-band excitation into the $^7F_{0,1} \rightarrow {}^5L_6$ transition was measured as a function of the Eu^{3+} concentration x ($0 < x \leqslant 1$) at 300 K. Figure 6 shows the results. It demonstrates that a strong quenching occurs at concentrations higher than $x = 0.1$. This is due to migration of the excitation energy over the Eu^{3+} sublattice to quenching impurities [1,13,16]. For two- and three-dimensional Eu^{3+} sublattices it was found that the critical concentration x_c obeys the empirical rule [17]

$$x_c = 2/N, \tag{4}$$

where N is the number of neighbouring positions on the sublattice to which transfer occurs. In view of the fact that the Eu^{3+} (S_6) $\rightarrow$ Eu^{3+} (C_2) energy transfer is very efficient, that there are three times more Eu^{3+} (C_2) ions than Eu^{3+} (S_6) ions and that the Eu^{3+} (C_2) ions are connected via superexchange contrary to the Eu^{3+} (S_6) ions, it is very reasonable to assume that the energy migration occurs over the Eu^{3+} (C_2) sublattice. The value of $x_c = 0.1$ leads to N is 20. From this value it can be calculated that the Eu^{3+} (C_2)–Eu^{3+} (C_2) interaction reaches as far as about 6 Å at 300 K. Every Eu^{3+} (C_2) ion has 18 neighbours within 6.1 Å.

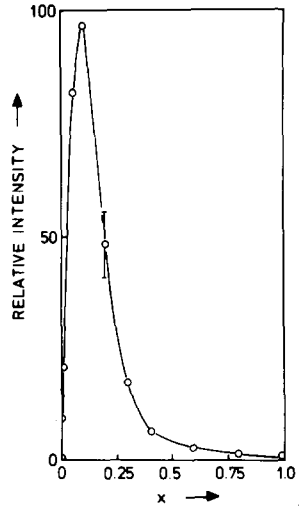

Fig. 6. Concentration dependence of the integrated Eu^{3+} emission intensity in $(Y_{1-x}Eu_x)_2O_3$ at 300 K (exc. = 394 nm).

3.3. Time dependence of the luminescence

The radiative decay times of the Eu^{3+} (S_6) and Eu^{3+} (C_2) ions were determined by measuring the $^5D_0$ emission decay of both types of ions after excitation into the $^5D_1$ level in a sample of composition $(Y_{0.999}Eu_{0.001})_2O_3$. The spectra of this sample showed that there is no observable interaction between the Eu^{3+} ions for this low Eu^{3+} concentration. After an initial buildup of about 100 μs, both decay curves become exponential in the temperature range under consideration. The buildup is due to relaxation from the $^5D_1$ level to the $^5D_0$ level. The risetime conforms very well to the lifetime of the $^5D_1$ level, which was found to decrease from 134 μs for 0.02% Eu^{3+} to 66 μs for 5% Eu^{3+} in Y_2O_3 due to cross relaxation [14]. The $^5D_0$ (C_2) decay time has a constant value of 1100 μs for the different temperatures, while the $^5D_0$ (S_6) decay time varies from 9600 μs at 1.3 K to 7900 μs at 300 K. These values agree with the radiative decay time values of 1000 μs and 7700 μs found by Forest and Ban [5] at 78 K for Eu^{3+} (C_2) and Eu^{3+} (S_6) in $(Gd_{0.994}Eu_{0.006})_2O_3$, respectively. The decrease of the S_6 decay time is probably due to an enhanced coupling with asymmet-

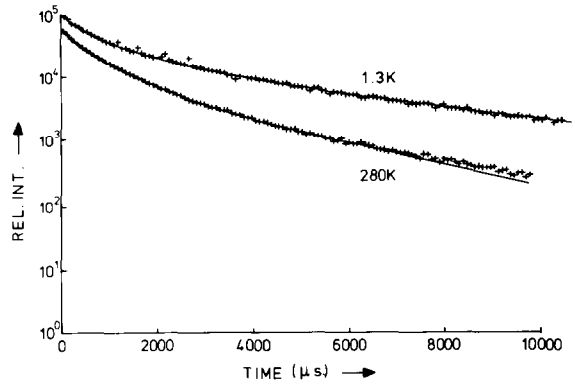

Fig. 7. Semilogarithmic decay curves of the $^5D_0 \rightarrow {}^7F_1$ Eu^{3+} (S_6) emission (em. = 582.00 nm) after excitation into the Eu^{3+} (S_6) ions (exc. = 523.54 nm) in $(Gd_{0.95}Eu_{0.05})_2O_3$, recorded at 1.3 K and 280 K. Solid lines: fits to eq. (6).

ric vibrations at higher temperatures, which induces electric dipole transitions on the Eu^{3+} (S_6) ion and lowers the lifetime of the $^5D_0$ (S_6) level. This is sustained by the fact that a weak $^5D_0 \rightarrow {}^7F_2$ line occurs at 611.5 nm in the emission spectrum of Eu^{3+} (S_6) in $(Y_{0.999}Eu_{0.001})_2O_3$ at 300 K which is not present at 4.2 K. The high value of the S_6 radiative decay time agrees with the fact that the transitions from $^5D_0$ (S_6) are magnetic dipole transitions.

For a detailed study of the energy transfer process from Eu^{3+} (S_6) to Eu^{3+} (C_2), the $^5D_0$ (S_6)

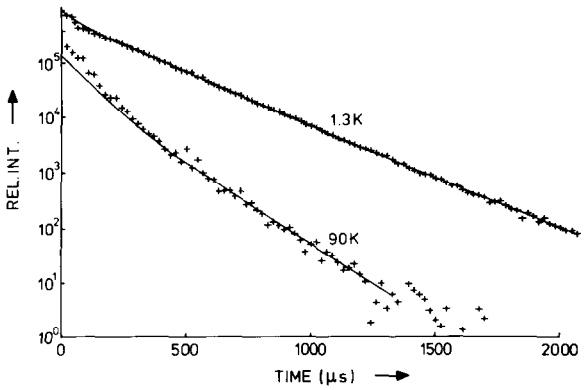

Fig. 8. Semilogarithmic decay curves of the $^5D_0 \rightarrow {}^7F_2$ Eu^{3+} (C_2) emission (em. = 611.3 nm) in Eu_2O_3, recorded at 1.3 K and 90 K. Solid lines: fits to eq. (17).

emission decay after excitation into the $^5D_1$ (S_6) level in a sample of composition $(Gd_{0.95}Eu_{0.05})_2O_3$ was used. It appeared to be non-exponential and faster than the radiative decay in the whole temperature range. Examples of such decay curves are given in fig. 7. It also shows that the decay time decreases on increasing temperature. The $^5D_1 - {}^5D_0$ relaxation is too fast to be noticed on the time scale under consideration. The $^5D_0$ (C_2) decay after excitation into the Eu^{3+} (S_6) ion shows a buildup reflecting the transfer process. It is the same buildup as found for the $^5D_0$ (C_2) decay after excitation into the $^7F_0 \rightarrow {}^5D_1$ (S_6) main line in $(Y_{0.95}Eu_{0.05})_2O_3$ [10].

Energy migration in Eu_2O_3 was investigated by using the $^5D_0$ (C_2) emission decay after excitation into the $^5D_1$ (C_2) level. Figure 8 shows two examples of such decay curves. At all temperatures the decay is faster than the radiative decay. It grows faster from 1.3 K to 90 K. Above 90 K the decay does not change anymore. The decay curves are initially non-exponential and become exponential after long times.

4. Discussion

4.1. $(Gd_{0.95}Eu_{0.05})_2O_3$

In view of the preceding results energy transfer from Eu^{3+} (S_6) to Eu^{3+} (C_2) is possibly due to take place by superexchange via the O^{2-} ligands: electric dipolar interaction is ruled out because electric dipole transitions are forbidden on the Eu^{3+} (S_6) ion and cooperative absorption indicates that superexchange occurs between the two types of ions.

Following the theory for the energy transfer process developed by Förster [18] and Dexter [19], Dornauf and Heber [20] derived an expression for the description of the donor decay in the case of superexchange. The transfer probability P for superexchange is given by

$$P = \frac{1}{\tau_0}\exp\left[\gamma(R_0 - R)\right], \qquad (5)$$

where τ_0 is the radiative decay time of the donor, γ is the exchange constant, R is the donor–

acceptor separation and R_0 is the critical transfer distance, for which the transfer rate is equal to the radiative decay rate. When the acceptor surroundings of the donor are described by a set of coordination shells l with radius ${}^lR$ and with ${}^lZ$ acceptor sites, the time development of the donor emission has the form [20]

$$I(t) = I_0 \exp\left(-\frac{t}{\tau_0}\right) \exp\left\{-\frac{t4\pi N_a}{\tau_0} \times\left(\frac{{}^{k+1}R^2}{\gamma} + 2\frac{{}^{k+1}R}{\gamma^2} + \frac{2}{\gamma^3}\right) \times\exp\left[\gamma\left(R_0 - {}^{k+1}R\right)\right]\right\} \times\left\{\sum_{l=1}^{k} \frac{{}^lZ}{Z}\exp\left(-\frac{t}{\tau_0}\exp\left[\gamma\left(R_0 - {}^lR\right)\right]\right)\right\}^{Zx}, \quad (6)$$

where I_0 is the intensity at $t = 0$, N_a is the number of acceptor ions per unit volume, x is the acceptor concentration and $Z = \sum_{l=1}^{k} {}^lZ$. k must be taken large enough, so that the total number of acceptors can be approximated by Zx and the overall transition probability to acceptors at ${}^{k+1}R$ is small compared to the radiative decay rate.

In $(Gd_{0.95}Eu_{0.05})_2O_3$ the donors are Eu^{3+} (S_6) ions, the acceptors Eu^{3+} (C_2) ions, τ_0 decreases from 9600 μs at 1.3 K to 7900 μs at 300 K, $N_a = 9.2 \times 10^{20}$ cm^{-3} and $x = 0.0375$. Using these values and the crystallographic data given by Wyckoff [12], the experimental decay curves were fitted to eq. (6) taking I_0, γ and R_0 as adjustable parameters. The set of radii used for the fitting ranged from 3.6 Å to 18.9 Å, containing 504 possible acceptor sites. Two examples of best fits are given in fig. 7 by the solid lines. The agreement with the experimental curves is excellent at all temperatures. Above 180 K a slight deviation occurs after long times which we ascribe to back transfer. At these temperatures the energy difference of 100 cm^{-1} (see fig. 4) between the $^5D_0$ levels of the Eu^{3+} (C_2) and Eu^{3+} (S_6) ions can be bridged by thermal activation.

From these fits R_0 occurred to vary from 7.3 Å at 1.3 K to 8.2 at 150 K. Above that temperature it does not change any more. It has the same order of magnitude as the critical transfer distance determined from the emission intensity. These results differ from those obtained by Köbler and Heber [7,8] for $(Y_{0.95}Eu_{0.05})_2O_3$. Although they arrived at a comparable value for R_0, viz. 8.7 Å, they found it to be independent of temperature. This is due to the fact that these authors did not take into account the distance dependence of the interaction.

The exchange constant γ has a value of 0.75 Å^{-1} and does not change up to 150 K. At higher temperatures it decreases to 0.56 Å^{-1} at 300 K. According to Dexter [19] γ is equal to $2/L$, where L is an effective average Bohr radius for the excited and unexcited states of the superexchange complex. This radius is 2.7 Å for $\gamma = 0.75$ Å^{-1} and 3.6 Å for $\gamma = 0.56$ Å^{-1}. Considering the fact that the sum of the ionic radii of O^{2-} and Eu^{3+} is 2.4 Å [11], this would imply that the superexchange occurs via more than one O^{2-} ligand above 150 K. However, this is a process with a low probability and will consequently not lead to a significant increase of the transfer probability.

Also an effective radius of 2.7 Å seems rather large for this superexchange system. This might be due to the fact that superexchange is not the only type of interaction between the Eu^{3+} (S_6) ions and the Eu^{3+} (C_2) ions. Another possibility is dipole–quadrupole interaction, where the quadrupole transition is on the Eu^{3+} (S_6) ion. Although the radiative transition probability for the quadrupole transition is usually too small to make any contribution to the radiative decay, it can be very important for nonradiative energy transfer [21]. The time development of the donor emission for dipole–quadrupole interaction between donor and acceptor is given by [22]

$$I(t) = I_0 \exp\left(-\frac{t}{\tau_0} - \Gamma\left(\tfrac{5}{8}\right)\frac{N_a}{c_0}\left(\frac{t}{\tau_0}\right)^{3/8}\right), \quad (7)$$

where c_0 is the critical transfer concentration given by

$$c_0^{-1} = \tfrac{4}{3}\pi R_0^3, \quad (8)$$

and

$$P\tau_0 = (R_0/R)^8. \quad (9)$$

P is the transfer probability for dipole–quadrupole interaction between donor and acceptor. It appeared that the fits of the $^5D_0$ (S_6) decay curves in $(Gd_{0.95}Eu_{0.05})_2O_3$ to eq. (7) are of the same quality as the fits to eq. (6), so that probably both types of interaction play a role in the transfer process. The fits to eq. (7) resulted in values of R_0 varying from 7.9 Å at 1.3 K to 9.2 Å at 300 K, being somewhat larger than for the superexchange interaction.

With the obtained values for R_0, the nearest neighbour Eu^{3+} (S_6) → Eu^{3+} (C_2) transfer probability ($R = 3.6$ Å) can now be calculated for both types of interaction using eqs. (5) and (9). The results are plotted as a function of temperature in fig. 9 for superexchange interaction and in fig. 10 for dipole–quadrupole interaction. The temperature dependence results from the large energy difference of 100 cm^{-1} between the $^5D_0$ (S_6) and the $^5D_0$ (C_2) level. This mismatch has to be overcome by phonon assistance. The two most probable forms of phonon assistance for the Eu^{3+} (S_6) to Eu^{3+} (C_2) transfer are schematically drawn in fig. 11. Figure 11a represents a direct one-phonon assisted process, where the mismatch is overcome by the emission of a phonon of 100 cm^{-1} at the S_6 site or at the C_2 site, while a one-site resonant two-phonon assisted process which will gain importance at higher temperatures is depicted in fig. 11b. Here the absorption of a phonon of 139 cm^{-1}, resonant with the $^7F_{1a}$–$^7F_0$ (S_6) energy difference, and the emission of a phonon of 239 cm^{-1} occur at the Eu^{3+} (S_6) site. Following the treatment of Holstein et al. [23] the transfer probability due to the one-phonon assisted process can be expressed by

$$P_{\mathrm{OPA}} \frac{J^2 \langle h^{\mathrm{I}} \rangle_{\Omega}^2 \Delta E_{12}}{2\pi\hbar^4 \rho v_t^5} (n(\Delta E_{12}) + 1), \qquad (10)$$

assuming the Debye approximation for the phonon density of states and taking the angular average of the strain tensor as unity. $J = \langle 1, 2^* | H | 1^*, 2 \rangle$ is the matrix element for the superexchange or dipole–quadrupole coupling between the two Eu^{3+} sites, ρ is the crystal density, v_t is the transverse velocity of sound, ΔE_{12} is the $^5D_0$ (S_6)–$^5D_0$ (C_2) energy difference, n is the Bose population factor and the coherence factor

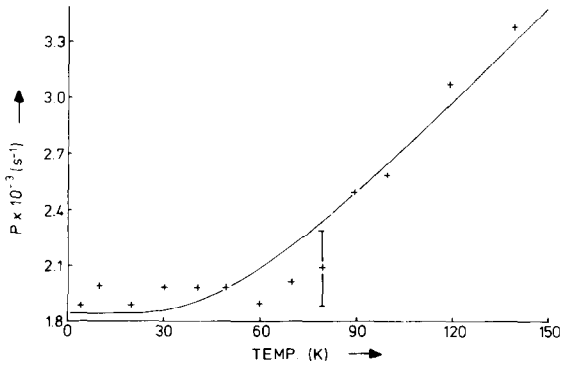

Fig. 9. Temperature dependence of the Eu^{3+} (S_6) → Eu^{3+} (C_2) transfer probability for superexchange interaction in $(Gd_{0.95}Eu_{0.05})_2O_3$. Solid line: fit to eq. (14).

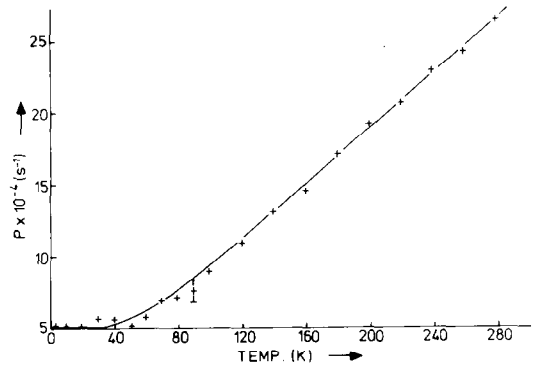

Fig. 10. Temperature dependence of the Eu^{3+} (S_6) → Eu^{3+} (C_2) transfer probability for dipole–quadrupole interaction in $(Gd_{0.95}Eu_{0.05})_2O_3$. Solid line: fit to eq. (14).

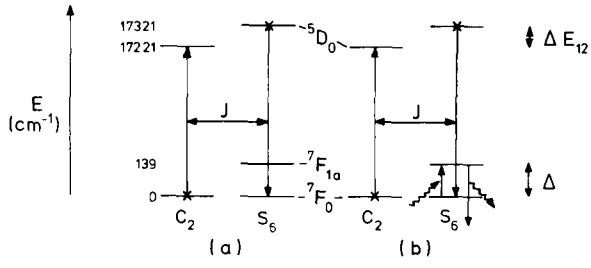

Fig. 11. Schematic diagram of the phonon assisted energy transfer processes occurring in $(Gd_{0.95}Eu_{0.05})_2O_3$. (a) Direct one-phonon assisted process, (b) one-site resonant two-phonon assisted process.

$\langle h^I \rangle_\Omega$ is given by

$$\langle h^I \rangle_\Omega = \Delta M^2(S_6) + \Delta M^2(C_2) - 2\Delta M(S_6)\Delta M(C_2)\frac{\sin qr}{qr}, \quad (11)$$

where $\Delta M(i)$ is the difference in ion–phonon coupling strength between ground and excited state for the Eu^{3+} ion on site i, q is the phonon wavevector and r the separation of the sites. Since ΔE_{12} is very large, eq. (11) reduces to

$$\langle h^I \rangle_\Omega = \Delta M^2(S_6) + \Delta M^2(C_2). \quad (12)$$

Similarly the expression for the two-phonon assisted process can be derived to be

$$P_{TPA} = \frac{3J^2A^2(\Delta + \Delta E_{12})^3}{2\pi\hbar^4\rho v_t^5(\Delta E_{12})^2}(n(\Delta + \Delta E_{12}) + 1) \times e^{-\Delta/kT}, \quad (13)$$

where A is the ion–phonon coupling strength between the $^7F_{1a}$ and $^7F_0$ states of the Eu^{3+} (S_6) ion and Δ is the energy difference between these levels.

The experimental transfer probability for both types of interaction fits well to the equation

$$P = \alpha_1(n(\Delta E_{12}) + 1) + \alpha_2(n(\Delta + \Delta E_{12}) + 1) \times e^{-\Delta/kT}, \quad (14)$$

as is illustrated in figs. 9 and 10. The solid line in fig. 9 corresponds to $\alpha_1 = 1.8 \times 10^3\ s^{-1}$ and $\alpha_2 = 1.7 \times 10^3\ s^{-1}$ and to $\alpha_1 = 5.0 \times 10^4\ s^{-1}$ and $\alpha_2 = 20 \times 10^4\ s^{-1}$ in fig. 10. From α_1 and α_2 the ratio of $\Delta M^2(S_6) + \Delta M^2(C_2)$ and A^2 can be calculated to be 40 for superexchange interaction and 10 for dipole–quadrupole interaction. Since the ion–phonon coupling strengths of excited and ground state, which are typically of the order of 1000 cm^{-1} for rare-earth transitions [23], will not be too different from each other, a cancellation will occur in $\Delta M(i)$. This implies that A has to be smaller than the coupling strengths of the ground and excited states. A further evaluation of these findings is not possible however, because no data are available on the strain in $Gd_2O_3:Eu^{3+}$.

The one-site resonant two-phonon assisted process is frequently encountered in rare-earth systems where a suitable resonant level is available in the temperature range under consideration [1,2,4, 24,25]. Except for very low temperatures, the direct one-phonon assisted process occurs seldom in rare-earth compounds because in most of these compounds energy transfer occurs between similar rare-earth ions which have small energy mismatches ΔE_{12} (in the order of some cm^{-1}) due to inhomogeneous broadening of the energy levels. For small energy mismatches between similar ions, where similar means that the $\Delta M(i)$'s are approximately the same for different sites i, the coherence factor $\langle h^I \rangle_\Omega$ becomes zero according to eq. (11). In combination with the small phonon density of states at low phonon energies this leads to a very small probability for the direct one-phonon process. Both restrictions do not apply for the Eu^{3+} (S_6) → Eu^{3+} (C_2) transfer, where the sites are different and the energy mismatch is large (100 cm^{-1}). Hence a one-phonon assisted process of the same magnitude as the two-phonon assisted process is not surprising.

This situation is contrary to the situation in β'-$Gd_2(MoO_4)_3:Eu^{3+}$. In the molybdate the energy mismatch between the different Eu^{3+} ions is very small [4]. Since the energy transfer between these ions could only be measured up to 50 K, no resonant level could be involved in the transfer process under study. The transfer was indeed found to occur by a two-site nonresonant two-phonon assisted process, which is the most probable process to occur under such circumstances [23].

4.2. Eu_2O_3

Figure 6 shows that energy migration occurs in Eu_2O_3 at 300 K. It was argued in section 3.2 that the energy migrates over the C_2 sublattice to quenching impurities. This migration persists down to 1.3 K, since even at that temperature the Eu^{3+} $^5D_0$ (C_2) emission decay is faster than the radiative decay.

The long-time exponentiality of the C_2 decay curves (see fig. 8) points to a three-dimensional diffusion-limited energy migration [26]. If we express the decay time of the exponential part of the curves by

$$\tau^{-1} = \tau_0^{-1} + \tau_D^{-1}, \quad (15)$$

where τ_D is the decay time due to migration, an expression for τ_D^{-1} for the case of dipolar donor–acceptor interaction has been derived [27]:

$$\tau_D^{-1} = 11.404\ N_a C^{1/4} D^{3/4} \tag{16}$$

where N_a is the number of acceptor ions (in this case impurity ions) per unit volume, C is the interaction parameter for donor–acceptor interaction and D is the diffusion constant. The whole decay is described by

$$I(t) = I_0 \exp\left(-\frac{t}{\tau_0}\right) \exp\left\{-\tfrac{4}{3}\pi^{3/2} N_a (Ct)^{1/2} \times \left(\frac{1 + 10.87x + 15.50x^2}{1 + 8.743x}\right)^{3/4}\right\}, \tag{17}$$

where $x = DC^{-1/3}t^{2/3}$. For $t \to \infty$ the expression between brackets transforms to the right-hand side of eq. (16).

Figure 8 shows two examples of fits of the experimental decay curves to eq. (17) (solid lines). At low temperatures the fits are in good agreement with the experimental curves, while at higher temperatures a deviation occurs at the beginning of the curves. Above 90 K no change occurs in the form of the decay curves. From the fits N_a was found to be about 2×10^{18} cm^{-3}, which is in good agreement with the nominal amount of impurities, viz. 2.5×10^{18} cm^{-3} ($\triangleq 0.01\%$). It proved much more difficult to find one unambiguous value for C and D for every curve. Depending on the initial values for the fitting parameters a whole set of combinations for C and D covering different orders of magnitude resulted in fits of comparable quality.

An independent way to determine the interaction strength C is given by Voronko et al. [28]. The nonexponential initial part of the decay curve reflects the direct donor–acceptor interaction. It should obey the relation

$$I(t) = I_0 \exp\left(-\frac{t}{\tau_0} - \beta t^{1/2} - \frac{t}{\tau}\right), \tag{18}$$

where τ is the decay time of the exponential long-time part of the decay curve, given by eq. (15), while β is given by

$$\beta = \tfrac{4}{3}\pi^{3/2} N_a C^{1/2} \tag{19}$$

for dipolar donor–acceptor interaction. Using I_0 and β as adjustable parameters, C was obtained by fitting the beginning of the decay curves to eq. (18). The resulting values are given by the crosses in fig. 12 as a function of temperature. The nonexponential part of the curves is very short, as can be seen from fig. 8. Since these curves were measured using the minimum channel width of the multichannel analyzer, viz. 10 μs, we were not able to study these parts in more detail. This is the reason for the large scatter in the values of C. The values for the diffusion constant given in fig. 12 by the circles were obtained from the C values and the exponential parts of the decay curves using eq. (16). Due to the large scatter in the C values resulting in a large scatter in the D values no conclusions can be drawn about the temperature dependence of the migration process.

The transfer probability between the Eu^{3+} (C_2) ions in Eu_2O_3 can be calculated using

$$P = 6D/a^2, \tag{20}$$

a is the distance between nearest neighbour Eu^{3+} (C_2) ions, viz. 3.6 Å. The average value of D is about 4×10^{-10} cm^2 s^{-1}, resulting in $P = 2 \times 10^6$ s^{-1}. This is one order of magnitude higher than was found for systems with comparable Eu^{3+} separation like $NaEuTiO_4$ [13] and EuOCl [29], viz. 3×10^5 s^{-1}, at low temperatures. It illustrates again the strong interaction between the Eu^{3+} ions in the sesquioxide system.

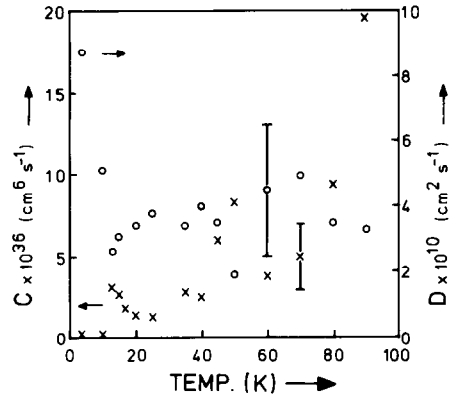

Fig. 12. Temperature dependence of the donor–acceptor interaction parameter C (crosses) and the diffusion constant D (circles) in Eu_2O_3.

The transfer probability from Eu^{3+} (C_2) to the impurities follows from [28]

$$P = C/a^6 \tag{21}$$

for dipolar interaction. If we assume that the impurity occupies a cation site, we can take a to be 3.6 Å. For $C = 1.5 \times 10^{-36}$ cm^6 s^{-1} (at 20 K) P becomes 7×10^8 s^{-1}. Since this is larger than the Eu^{3+} (C_2) $\rightarrow$ Eu^{3+} (C_2) transfer probability, the assumption of diffusion limited energy migration seems to be reasonable.

The fact that the Eu^{3+} (C_2) decay does not become faster at temperatures above 90 K is very peculiar. This is opposite to the situation in most concentrated Eu^{3+} systems, where the decay rate increases in the whole temperature range under consideration, the transfer between Eu^{3+} ions being phonon assisted. A possible explanation for the decay behaviour in Eu_2O_3 is that at higher temperatures the Eu^{3+} (C_2) ions have the possibility to transfer their energy to Eu^{3+} (S_6) ions. This process is thermally activated over an energy of 100 cm^{-1}. Although the back transfer is very efficient, it means that the excitation energy migrating through the Eu^{3+} (C_2) sublattice will be trapped for a certain time by the Eu^{3+} (S_6) anti-traps. Due to the large amount of Eu^{3+} (S_6) ions, this will slow down the migration. The thermal activation of the anti-trapping may neutralize the increase in transfer rate between the Eu^{3+} (C_2) ions. This process is then responsible for the discrepancy between the fit to eq. (17) and the experimental decay curve at 90 K. It is however very difficult to convert this into a quantitative model.

In conclusion, we can say that analogous to what we found for the energy transfer in β'-$Gd_2(MoO_4)_3 : Eu^{3+}$, it is very difficult to describe the energy transfer processes in the concentrated Eu^{3+} system accurately. This is mainly due to the complexity of the system, brought about by the two different crystallographic sites and by the presence of quenching impurities. On the other hand a clear analysis of the transfer processes in the diluted $Gd_2O_3 : Eu^{3+}$ and $Y_2O_3 : Eu^{3+}$ compounds is possible. While the nature of the acceptors (impurities) and strength of donor–acceptor interaction in the concentrated compound remain difficult to reveal, the dilution offers a system where all the relevant parameters can be assigned. In the diluted compound the impurities have no influence because the excitation energy cannot reach them by energy migration as in the concentrated compound.

Acknowledgement

The investigations were supported by the Netherlands Foundation for Chemical Research (SON) with financial aid from the Netherlands Organisation for Advancement of Pure Research (ZWO).

References

[1] M. Buijs and G. Blasse, J. Lumin. 34 (1986) 263.
[2] M. Buijs, J.P.M. van Vliet and G. Blasse, J. Lumin. 35 (1986) 213.
[3] P.A.M. Berdowski, M. Buijs and G. Blasse, J. Physique C 7 (1985) 31.
[4] M. Buijs, G. Blasse and L.H. Brixner, Phys. Rev. B 34 (1986) 8815.
[5] H. Forest and G. Ban, J. Electrochem. Soc. 116 (1969) 474.
[6] J. Heber, K.H. Hellwege, U. Köbler and H. Murmann, Z. Phys. 237 (1970) 189.
[7] U. Köbler, Z. Phys. 250 (1972) 217.
[8] J. Heber and U. Köbler, in: Luminescence of Crystals, Molecules and Solutions, ed. F. Williams (Plenum Press, New York, 1973) p. 379.
[9] R.G. Pappalardo and R.B. Hunt Jr., J. Electrochem. Soc. 132 (1985) 721.
[10] R.B. Hunt Jr. and R.G. Pappalardo, J. Lumin. 34 (1985) 133.
[11] R.D. Shannon, Acta Cryst. A32 (1976) 751.
[12] R.W.G. Wyckoff, in: Crystal Structures, Vol. 2. (Wiley & Sons, New York, 1963).
[13] P.A.M. Berdowski and G. Blasse, J. Lumin. 29 (1984) 243.
[14] A.T. Rhys Williams and M.J. Fuller, Computer Enhanced Spectr. 1 (1983) 145.
[15] S. Imanaga, S. Yokono and T. Hoshina, J. Lumin. 16 (1978) 77.
[16] P.A.M. Berdowski, R. van Mens and G. Blasse, J. Lumin. 33 (1985) 147.
[17] P.A.M. Berdowski and G. Blasse, J. Solid State Chem. 63 (1986) 86.
[18] T. Förster, Ann. Phys. 2 (1948) 55.
[19] D.L. Dexter, J. Chem. Phys. 21 (1953) 836.
[20] H. Dornauf and J. Heber, J. Lumin. 22 (1980) 1.
[21] R.K. Watts, in: Optical Properties of Ions in Solids, ed. B. Di Bartolo (Plenum Press, New York, 1975) p. 307.

[22] M. Inokuti and F. Hirayama, J. Chem. Phys. 43 (1965) 1978.
[23] T. Holstein, S.K. Lyo and R. Orbach, in: Laser Spectroscopy of Solids, eds. W.M. Yen and P.M. Selzer (Springer, Berlin, 1981) Chap. 2.
[24] L.D. Merkle and R.C. Powell, Phys. Rev. B 20 (1979) 75.
[25] J.R. Wietfeldt, D.S. Moore, B.M. Tissue and J.C. Wright, Phys. Rev. B 33 (1986) 5788.
[26] D.L. Huber, Chap. 3 in ref. [23]
[27] M. Yokota and N. Tanimoto, J. Phys. Soc. Japan 22 (1967) 779.
[28] Y.K. Voronko, T.G. Mamedov, V.V. Osiko, A.M. Brochorov, V.P. Sakuu and I.A. Shcherbakov, Sov. Phys. JETP 44 (1976) 251.
[29] P.A.M. Berdowski, J. van Herk and G. Blasse, J. Lumin. 34 (1985) 9.